Radiative transfer in the O 2 A-band - a fast and accurate forward model based on the ℓ -distribution approach

Frédéric André, C. Cornet, Mathieu Galtier, Ph. Dubuisson

Radiative transfer in the O 2 A-band – a fast and accurate forward model based on the ℓ -distribution approach

Article *in* Journal of Quantitative Spectroscopy and Radiative Transfer · December 2020

DOI: 10.1016/j.jqsrt.2020.107470

CITATIONS
0

READS
35

4 authors:

Frédéric André
Institut National des Sciences Appliquées de Lyon
125 PUBLICATIONS **666** CITATIONS
SEE PROFILE

Celine Cornet
Université de Lille
80 PUBLICATIONS **1,114** CITATIONS
SEE PROFILE

Mathieu Galtier
Institut National des Sciences Appliquées de Lyon
37 PUBLICATIONS **198** CITATIONS
SEE PROFILE

P. Dubuisson
Université de Lille
167 PUBLICATIONS **2,918** CITATIONS
SEE PROFILE

Radiative transfer in the O_2 A-band - a fast and accurate forward model based on the ℓ-distribution approach

André, F.[a,*], Cornet, C.[b], Galtier, M.[a], Dubuisson, Ph.[b]

[a] *Univ Lyon, CNRS, INSA-Lyon, Université Claude Bernard Lyon 1, CETHIL UMR5008, F-69621 Villeurbanne, France*
[b] *Univ. Lille, CNRS, LOA UMR8518, F-59655, Villeneuve d'Ascq, France*

Abstract

An efficient method based on accurate transmissivity calculations to account for gaseous absorption in Monte Carlo / quasi-Monte Carlo radiative transfer codes is presented. The modeling approach is based on an improved non-uniform transmission formulation, called the ℓ-distribution method. The technique is founded on two components: 1/ an original uniform method to tabulate band averaged transmissivities of gaseous paths and 2/ its extension to non-uniform paths, based on the Godson-Weinreb-Neuendorffer's (GWN) approximation that consists of the definition of effective scaling factors to relate gaseous spectra in distinct states. As the GWN method is known to provide results dependent on the ordering of the gas layers, two path reordering strategies are introduced and compared. One of them is founded on results from statistical theory and requires the introduction of a new coefficient (Kendall's $\mathcal{K}e$). This coefficient together with its role on the path reordering strategy is introduced, detailed and analyzed. The two schemes are then assessed against Line-By-Line calculations in line-of-sight geometries. Two configurations representative of radiative transfer in the O_2 A-band for scattering atmospheres are then studied: the first one only considers molecular (Rayleigh) scattering and the second one involves various cloud configurations (single or bi-layer clouds located at

*Corresponding author
Email address: frederic.andre@insa-lyon.fr (André, F.)

various altitudes). For these calculations, the ℓ-distribution methods based on the two path reordering schemes were implemented in the 3D Monte Carlo code 3DMCPOL. Results of the ℓ-distribution method are compared with solutions provided by the Correlated k-distribution method and assessed against Line-By-Line calculations. The ℓ-distribution approach combined with the Kendall's reordering strategy is shown to provide results more accurate than k-distributions at smaller calculation costs. The ℓ-distribution method is shown to be a relevant candidate for radiative transfer in the atmosphere, both for remote sensing applications but also for weather forecasting or radiative budget studies, with or without scattering phenomena.

Keywords: remote sensing, O_2 A-band, scattering atmosphere, ℓ-distribution, k-distribution, LBL

---

1. Introduction

Satellite and ground based imaging devices are widely used in remote sensing applications for the inference of atmospheric parameters from radiance (reflected and/or emitted) measurements. The reliability of the inferred atmospheric profiles (temperature, species concentrations, *etc*) strongly depends on the accuracy of the forward radiation model used in combination with the inversion method. The most accurate technique to account for gaseous absorption in the simulation of radiative transfer processes in the atmosphere is the Line-By-Line (LBL) method [1, 2]. But this technique, even if some optimized versions such as 4A/OP (Automatized Atmospheric Absorption Atlas) exist [3], is widely recognized as time-consuming which prevents its use in many practical problems, especially for operational calculus. Efficient though accurate parameterizations for the treatment of gaseous absorption remain of primary importance in atmosphere sciences, both in an operational context at a time where the amount of data produced by remote sensing devices increases exponentially, or for other applications, such as weather forecasting or radiative budget studies.

The high computational cost of LBL calculations is caused by the double

integration scheme required to evaluate band averaged transmissivities of non-uniform paths: 1/ a path integration is first needed to account for local contributions of the gaseous species encountered along the radiation path. Path integrals need to be evaluated for each wavenumber ν inside the spectral band of interest and, 2/ a spectral integration needs to be performed in order to average the contributions of all spectral values inside the considered band. This double integration scheme, and more critically the first one as it needs to be performed for each wavenumber, is the main source of computational cost in LBL calculations. It should be noticed that inversion of measured spectral data requires iterative schemes, associated with the minimization process of a cost function. This makes LBL calculation cost even more critical in this particular application context, since all path integrals need to be evaluated many times during the exploration of the parameter search space before to reach the optimal solution. Presently, k-distribution methods [4] are among the most widely used approximate techniques to treat gaseous absorption. These approaches allow reducing significantly the amount of path integrals required to estimate band averaged radiances from thousands in the LBL approach to a few dozens in k-distributions. k-distribution methods require assumptions to treat path non-uniformities. These assumptions are their main source of errors in radiative transfer applications, with orders of magnitude of errors usually reported on the literature of a few percents in non-uniform cases [5].

In order to circumvent this problem of multiple integration, encountered in LBL but also to a less extent in k-distribution models, the ℓ-distribution method was proposed recently [6]. The approach, which was initially developed and applied in high temperature combustion applications, is the main focus of the present paper. This method is highly computationally efficient because it neither requires spectral or spatial integration schemes to estimate band averaged transmission functions of non-uniform gaseous paths. This results in a very fast direct model that can nevertheless achieve LBL accuracy both in uniform and non-uniform situations.

Up to now, most of the application cases reported in the literature for this

method were dedicated to high temperature applications, including standard line-of-sight benchmarks and turbulence-radiation interactions calculations in [6], and to radiative heat transfer simulations in benchmark [7] and actual tri-dimensional industrial (glass furnace geometries) configurations [8]. The aim of the present work is to evaluate this technique for atmospheric calculations by simulating reflectance at the top of the atmosphere, for different incident and satellite viewing angles, and for typical atmospheres composed of gaseous molecules and / or clouds.

The paper is structured as follows. The second section is dedicated to a description of the treatment of uniform gaseous paths by the ℓ-distribution approach. The third section focuses on the extension of the uniform approach to non-uniform paths. This adaptation of the method is founded on an application of the Godson-Weinreb-Neuendorffer's (GWN) method which consists in the definition of effective scaling factors. This method is recasted within the frame of Archimedean copula's theory to analyse some of its propertie.s The link between these mathematical properties and their physical interpretation is provided. The use of recent results from copula theory to improve the GWN method is the main originality of the present work. Section 4 is dedicated to applications of the method in clear sky and scattering atmosphere configurations. Absorption by a single molecular specie (O_2) is considered all along the paper.

2. The ℓ-distribution method in uniform gaseous layers

In this section, we introduce the main equations required to apply the ℓ-distribution method for the calculation of transmissivities of uniform atmospheric paths averaged over the spectral response function of an optical filter $\phi(\nu)$. Only the main results are given. Interested readers will find more details and explanations about the method in Refs. [6, 9].

We start with the gaseous transmittance of a single gas (as considered all along the present paper) in a uniform layer defined as:

$$\tau_{\phi}^{\Delta\nu}(L) = \frac{1}{\Phi} \int_{\Delta\nu} \phi(\nu) \exp(-\kappa_{\nu} L)\, d\nu \tag{1}$$

where $\tau_{\phi}^{\Delta\nu}(L)$ is the band averaged gaseous transmittance weighted by the filter reponse function $\phi(\nu)$, L (in cm) the total length of the gas path inside the uniform layer, κ_{ν} (in cm^{-1}) the spectral absorption coefficient of the gas inside the uniform layer at wavenumber ν (in cm^{-1}) and Φ the integral of the filter response function over the band $\Delta\nu$, $viz.$ $\Phi = \int_{\Delta\nu} \phi(\nu)\, d\nu$.

The ℓ-distribution approximation of the transmittance given by Eq. (1) can be written as:

$$\tau_{\phi}^{\Delta\nu}(L) = Gr\left[\tau_{0,\phi}^{\Delta\nu}(L)\right] \tag{2}$$

where $\tau_{0,\phi}^{\Delta\nu}(L)$ is called the "germ" model and Gr is a mapping function that associates values of the germ model for a given L with the true LBL transmittance at the same length. The germ model needs to be chosen in such a way that analytical mathematical expressions exist for both the transmissivity $\tau_{0,\phi}^{\Delta\nu}(L)$ and its inverse $\Lambda_{0,\phi}^{\Delta\nu}(X), X \in [0,1]$ defined as $\Lambda_{0,\phi}^{\Delta\nu}\left[\tau_{0,\phi}^{\Delta\nu}(L)\right] = L$. A simple choice for the germ is thus the Statistical Narrow Band model for Lorentz lines with the Malkmus' distribution of linestrengths (written from now on SNB-LM), $viz.$:

$$\tau_{0,\phi}^{\Delta\nu}(L) = \exp\left[-\frac{\beta}{\pi}\left(\sqrt{1+\frac{2\pi k_P L}{\beta}}-1\right)\right] \tag{3}$$

where k_P is the mean absorption coefficient of the gas weighted by the filter response function:

$$k_P = \frac{1}{\Phi} \int_{\Delta\nu} \phi(\nu)\, \kappa_{\nu}\, d\nu \tag{4}$$

Parameter β, that represents an overlapping parameter in the SNB-LM [10], only plays here the role of a coefficient that adjusts the curve-of-growth of the germ model at the optically thick limit. This parameter β is defined as:

$$\beta = \frac{1}{k_P/k_R - 1} \tag{5}$$

where we have introduced a band averaged Rosseland mean absorption coefficient k_R as:

$$\frac{1}{k_R} = \frac{1}{\Phi} \int_{\Delta\nu} \frac{\phi(\nu)}{\kappa_{\nu}}\, d\nu \tag{6}$$

The inverse $\Lambda_{0,\phi}^{\Delta\nu}(X)$ of the transmission function (3) is given analytically as:

$$\Lambda_{0,\phi}^{\Delta\nu}(X) = \frac{\beta}{2\pi k_P}\left[\left(1-\frac{\pi}{\beta}\ln X\right)^2 - 1\right] \tag{7}$$

From these definitions, one can immediatly notice that the mapping function, Gr, is simply given as:

$$Gr(X) = \frac{1}{\Phi}\int_{\Delta\nu}\phi(\nu)\exp\left[-\kappa_\nu \Lambda_{0,\phi}^{\Delta\nu}(X)\right]\,d\nu \tag{8}$$

The role of function Gr is to associate values of the germ model at a given value of the gas path length L, which provides some rough estimate of the true LBL transmissivity, to its actual LBL value. Gr maps the unit interval $[0,1]$ into itself and can be readily tabulated at any desired accuracy by: 1/ discretizing the interval $[0,1]$, 2/ estimating the function at the corresponding $X \in [0,1]$ by a direct application of Eq. (8) to the LBL dataset. Then, as soon as the look-up table $\{X_i, Gr(X_i)\}, i = 1,..,n$ is built, simple linear interpolations can be used to estimate values of Gr not included in the table. This tabulation process only needs to be done once for any set of thermophysical states of the gas and/or filter response functions. Basically, the uniform method used in the ℓ-distribution method thus consists of a tabulation of LBL data in terms of band averaged transmissivities instead of absorption coefficients. One part of the time-consuming process of LBL calculations (spectral integrals) is thus precalculated in advance which leads to a gain in terms of computation cost during the application of the model in radiative heat transfer calculations.

Examples of Gr functions for the O_2 A-band are plotted in Figure 1. From this figure, one can notice that Gr functions associated with layers near the ground (dotted curve, for a Mid-Latitude Summer (MLS) profile [11] at an altitude of 1 km viz. a total pressure of 1013 hPa and a temperature of 294 K) are close to the identity line ($Y = X$): this can be explained by the fact that for the layers found at the bottom of the atmosphere, as line profiles are mostly in the Lorentz regime, the germ model is very similar to the true LBL transmission curve. At the top of the atmosphere (TOA), on the other hand, line profiles are mostly Doppler. The corresponding Gr functions (plain curve, for a MLS profile

at an altitude of 120 km viz. a total pressure of 2.10^{-5} hPa and a temperature of 380 K) for high values of the transmissivities (X close to 1) are far from the identity line. This is because at this optically thin limit, large errors can be observed while trying to estimate transmissivities in the Doppler-dominant regime by a model for Lorentz lines.

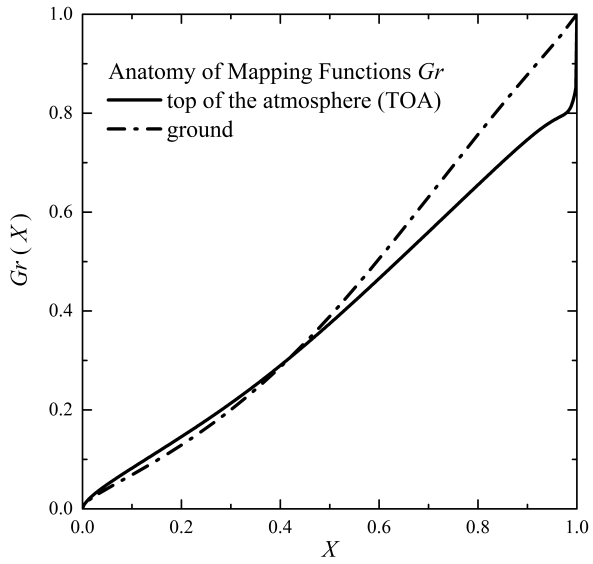

Figure 1: Anatomy of mapping functions Gr – parameter X represents the value of the germ function, that contains the information on the gas path length.

One interesting feature of this formulation in terms of mapping function Gr is that as Gr is strictly increasing, its inverse Gr^{-1} exists. This function can be obtained easilly by reverting the look-up table of the Gr function. This allows obtaining the inverse of function $\tau_{\phi}^{\Delta\nu}(L)$, written ℓ and defined through the relationship $\ell \circ \tau_{\phi}^{\Delta\nu}(L) = L$ as:

$$\ell(X) = \Lambda_{0,\phi}^{\Delta\nu}\left[Gr^{-1}(X)\right] \tag{9}$$

The ℓ-distribution method is probably the first approach to allow simultane-

ously estimating the direct model (band averaged transmissivity) and its inverse. This inverse ℓ can be used to construct a large range of possible models for the extension of the ℓ-distribution technique from uniform to non-uniform situations. Indeed, in the case of n distinct thermophysical states represented by a sequence $\kappa_\nu^1, .., \kappa_\nu^n$ of spectral absorption coefficients and for a set $L_1, .., L_n$ of pathlengths, the band averaged transmissivity of the non-uniform path $\tau_{1..n}^{\Delta\nu}(L_1, .., L_n)$ (from now on, we will simplify the general notation, which considers a filter response function, for legibility but application cases described later in this paper will account for its effect) defined as:

$$\tau_{1..n}^{\Delta\nu}(L_1, .., L_n) = \frac{1}{\Delta\nu} \int_{\Delta\nu} \exp(-\kappa_\nu^1 L_1 + .. + \kappa_\nu^n L_n)\, d\nu \tag{10}$$

can be written under the following mathematical form:

$$\tau_{1..n}^{\Delta\nu}(L_1, .., L_n) = \mathcal{C}_{1..n}\left[\tau_1^{\Delta\nu}(L_1), .., \tau_n^{\Delta\nu}(L_n)\right] \tag{11}$$

where $\mathcal{C}_{1..n}$ is a n-dimensional copula given in terms of functions $\ell_i, i = 1, .., n$ as:

$$\mathcal{C}_{1..n}(X_1, .., X_n) = \frac{1}{\Delta\nu} \int_{\Delta\nu} \exp\left[-\kappa_\nu^1 \ell_1(X_1) + .. + \kappa_\nu^n \ell_n(X_n)\right]\, d\nu \tag{12}$$

This formulation was successfully applied in high temperature configurations in Ref. [12] for dimension up to $n = 4$ based on multivariate polynomial representations of function $\mathcal{C}$. For higher dimensions, polynomial expressions can quickly require a large amount of coefficients and become computationally inefficient both in terms of calculation cost (which increases with the number and orders of the polynomials) and memory space (to store the polynomial coefficients): the use of neural networks is then recommended. Such developments are scheduled as future work but are not considered further in the following.

Another possible use of function ℓ is its application to the GWN (Godson-Weinreb-Neuendorffer, see [10]) method which is detailed in the next section.

3. Adaptation of ℓ-distributions to non-uniform gaseous paths through the GWN method

The GWN method is among the oldest non-uniform techniques. It was first proposed by Godson in 1953 [13], two years before the widely used Curtis-Godson approximation [14, 10]. The same method was "rediscovered" independently in 1973 by Weinreb and Neuendorffer [15] and, in 1981, by Gordley and Russel [16] who called it the Emissivity Growth Approximation (EGA). More recently, Modest used the same technique within the frame of the k-distribution method and called it the scaled-k approximation [17]. Recent applications of the GWN method (called in this reference the EGA technique) in atmospheric configurations can be found in [18].

The GWN method can be rather naturally introduced as a generalization of scaled models. This is the aim of the next section. Connections with the theory of Archimedean copulas are also emphasized.

3.1. Scaled models and Archimedean copulas

We consider two spectra κ_ν^1 and κ_ν^2 associated with two gas layers in distinct thermophysical states. Layers are represented by exponents 1 and 2 respectively. The length of the gas path in state 1, at temperature T_1, is L_1 and that in state 2, at temperature T_2, is L_2. The transmissivity of the non-uniform path $L_1 + L_2$ is defined as:

$$\tau_{12}^{\Delta\nu}(L_1, L_2) = \frac{1}{\Delta\nu} \int_{\Delta\nu} \exp(-\kappa_\nu^1 L_1 - \kappa_\nu^2 L_2)\, d\nu \tag{13}$$

As the transmissivities of the uniform layers $\tau_1^{\Delta\nu}(L_1)$ and $\tau_2^{\Delta\nu}(L_2)$ are strictly decreasing with respect to L_1 and L_2, their inverses ℓ_1 and ℓ_2 defined as solutions of $\ell_i \circ \tau_i^{\Delta\nu}(L_i) = L_i, i = 1, 2$, exist. Equation Eq. (13) can be rewritten in terms of these inverses to provide:

$$\tau_{12}^{\Delta\nu}(L_1, L_2) = \mathcal{C}_{12}\left[\tau_1^{\Delta\nu}(L_1), \tau_2^{\Delta\nu}(L_2)\right] \tag{14}$$

where function $\mathcal{C}_{12}$ is defined for $X, Y \in [0, 1]$ as:

$$\mathcal{C}_{12}\left(X,Y\right)=\frac{1}{\Delta\nu}\int_{\Delta\nu}\exp\left[-\kappa_{\nu}^{1}\ell_{1}(X)-\kappa_{\nu}^{2}\ell_{2}(Y)\right]\,d\nu \tag{15}$$

It can be readily checked from its definition that function $\mathcal{C}_{12}$ has the following properties:

$$\mathcal{C}_{12}(X=1,Y)=Y,\,\mathcal{C}_{12}(X,Y=1)=X \tag{16}$$

$$\mathcal{C}_{12}(X=0,Y)=\mathcal{C}_{12}(X,Y=0)=0 \tag{17}$$

$$\frac{\partial^{2}\mathcal{C}_{12}(X,Y)}{\partial X\partial Y}\geq 0 \tag{18}$$

Accordingly, function $\mathcal{C}_{12}$ is mathematically called a copula [19]. It is important to notice here that the introduction of the concept of copula is only useful to clarify the type of function that relates the transmissivity of uniform paths to those of non-uniform layers. A detailed knowledge of copula's theory is not required to follow the next developments. Some useful definitions and theorems related to copula theory are provided in Reference [19].

The set of equations Eqs. (16) to (18) can be interpreted physically. Indeed, a value of X or Y equal to 1 indicates that the length of one of the two layers is zero ($\ell_i(1)=0$). In this case, the property given by Eq. (16) simply means that the application of function $\mathcal{C}_{12}$ to the couple of transmissivities provides the transmissivity of the layer with non-nul length. In a similar way, if one of the values of X or Y is equal to zero, this means that one of the gas paths has an infinite length ($\ell_i(0)=+\infty$) in which case the transmissivity of the non-uniform paths needs to be zero: this is actually what is meant by Eq. (17). In order to interpret physically the inequality (18), we need to introduce the next exchange $\varphi_{\delta L_1\leftrightarrow\delta L_2}$ between two small path elements δL_1 and δL_2 defined as:

$$\varphi_{\delta L_1\leftrightarrow\delta L_2}=\frac{\partial^{2}\tau_{12}^{\Delta\nu}(L_1,L_2)}{\partial L_1\partial L_2}\delta L_1\delta L_2\left[I_{b,\nu}(T_2)-I_{b,\nu}(T_1)\right] \tag{19}$$

where:

$$\frac{\partial^2 \tau_{12}^{\Delta\nu}(L_1, L_2)}{\partial L_1 \partial L_2} = \frac{1}{\Delta\nu} \int_{\Delta\nu} \kappa_\nu^1 \kappa_\nu^2 exp\left(-\kappa_\nu^1 L_1 - \kappa_\nu^2 L_2\right) d\nu \geq 0 \tag{20}$$

The sign of $\varphi_{\delta L_1 \leftrightarrow \delta L_2}$ thus only depends on the difference $[I_{b,\nu}(T_2) - I_{b,\nu}(T_1)]$. Consequently, it is positive if $T_2 \geq T_1$ indicating that the transfer of radiative energy arises in the direction of decreasing temperatures. Eq. (20) can be rewritten in terms of function $\mathcal{C}_{12}$:

$$\frac{\partial^2 \tau_{12}^{\Delta\nu}(L_1, L_2)}{\partial L_1 \partial L_2} = \frac{\partial \tau_1^{\Delta\nu}(L_1)}{\partial L_1} \frac{\partial \tau_2^{\Delta\nu}(L_2)}{\partial L_2} \frac{\partial^2 \mathcal{C}_{12}\left[X = \tau_1^{\Delta\nu}(L_1), Y = \tau_2^{\Delta\nu}(L_2)\right]}{\partial X \partial Y} \tag{21}$$

which is positive if and only if the joint derivative of $\mathcal{C}_{12}$ with respect to X and Y is strictly positive i.e. if Eq. (18) is true. Consequently, Eq. (18) can be interpreted as a condition that ensures the sign of net exchanges between gaseous cells to be properly evaluated when formulated in terms of function $\mathcal{C}_{12}$. It should be noticed at this level that if the "copula" property of function $\mathcal{C}_{12}$ can be easilly justified physically in the bi-variate case, the more general situation of n layers cannot be, unfortunately, interpreted in the same simple way.

If gas spectra are *scaled*, then the ratio $u = \frac{\kappa_\nu^2}{\kappa_\nu^1}$ does not depend on wavenumber, ν. Then, the previous equation simplifies into:

$$\tau_{12}^{\Delta\nu}(L_1, L_2) = \frac{1}{\Delta\nu} \int_{\Delta\nu} \exp\left[-\kappa_\nu^1 (L_1 + uL_2)\right] \, d\nu = \tau_1^{\Delta\nu}(L_1 + uL_2) \tag{22}$$

and the transmissivity of the non-uniform path can thus be treated exactly in the same way as the transmissivity of the gas in state 1 with a total length $L_1 + uL_2$ (a symetrical relationship can also be written in terms of state 2). In this situation, it thus suffices to know how to calculate average gas radiative transmissivities of uniform layers to treat any non-uniform situation.

Equation (22) can be rewritten in terms of the inverse ℓ_1 of the transmission function of the gas in state 1 defined by the relationship $\ell_1 \circ \tau_1^{\Delta\nu}(L_1) = L_1$ providing:

$$\tau_{12}^{\Delta\nu}(L_1, L_2) = \mathcal{C}_{11}\left[\tau_1^{\Delta\nu}(L_1), \tau_2^{\Delta\nu}(L_2)\right] \tag{23}$$

If gas spectra are scaled, the copula $\mathcal{C}_{12} = \mathcal{C}_{11}$ thus only depends on a single thermophysical state (state 1 in the considered case) and the copula is called *Archimedean*. Archimedean copulas are among the most widely used copula models because of their relatively simple extension to high dimensions.

In practice there exist two main physical reasons that explain the departure of gas spectra from *scaling*:

- gas spectra are made of many thin spectral lines whose profiles depend non-linearly on the local gas properties (temperature, pressure, species concentrations).

- the content of gas spectra (amount of single lines that participate to the value of the absorption coefficient at some given wavenumber ν) varies significantly with temperature. This is because linestrengths (surface of a single line calculated over its spectral profile) vary exponentially with respect to the temperature of the gas through a Boltzmann law.

Accordingly, the definition of a constant scaling coefficient is not physically realistic in the case of real gaseous media. Nevertheless, the use of Equation Eq. (23) remains possible, as a mean to relate the transmissivity of the non-uniform path to those of the uniform sub-layers. This is the principle of the GWN method. Indeed, this technique mostly consists of the definition of effective scaling coefficients that depend on the length of the gas paths through the relationship $u(L_2) = \frac{\ell_1 \circ \tau_2^{\Delta\nu}(L_2)}{L_2}$ [6, 20]. A detailed physical analysis of the concept of effective scalling factor is given in Ref. [20]. With this notation, it is in fact easy to check that:

$$\tau_{12}^{\Delta\nu}(L_1, L_2) = \mathcal{C}_{11}\left[\tau_1^{\Delta\nu}(L_1), \tau_2^{\Delta\nu}(L_2)\right] = \tau_1^{\Delta\nu}\left[L_1 + u(L_2)\, L_2\right] \tag{24}$$

which is similar to Eq.(22). But, instead of a constant scaling coefficient, an effective scaling factor that can be defined as solution of $\tau_2^{\Delta\nu}(L_2) = \tau_1^{\Delta\nu}\left[u(L_2)\, L_2\right]$

appears.

In general, the two copulas $\mathcal{C}_{11}$ and $\mathcal{C}_{22}$ are different and their application to the same couple of transmissivities $\tau_1^{\Delta\nu}(L_1)$ and $\tau_2^{\Delta\nu}(L_2)$ has no reason to provide the same result. Criteria thus needs to be defined in order to choose the "best direction" *viz.* the index $i = 1$ or 2 that provides the most physically realistic approximation of $\mathcal{C}_{12}$ by the Archimedean copula $\mathcal{C}_{ii}$. The choice of such a criterion is the objective of the next section.

3.2. Physical requirements for a reordering of the path

Let us consider an assembly of spectral lines inside a band $\Delta\nu$ whose centers: 1/ are statistically independent from each other and 2/ do not depend on the thermophysical state of the gas (line shift is thus not considered). For a non-uniform path made of n uniform layers of lengths $L_i, i = 1, .., n$ over each of which absorption coefficients constructed with the help of the preceeding set of lines can be found, the derivative of the transmissivity of the non-uniform path with respect to any $L_i, i = 1, .., n$ follows the following inequality:

$$-\frac{\partial \tau_{1..n}^{\Delta\nu}(L_1, .., L_n)}{\partial L_i} \leq k_P^i \; \tau_{1..n}^{\Delta\nu}(L_1, .., L_n) \tag{25}$$

This inequality on the spatial derivative of the mean equivalent width, given as $-\ln\left[\tau^{\Delta\nu}(L)\right]$, is rather common in the litterature of band models based on transmissivities [10]. However, the treatment proposed here introduces two subtleties. The first one is that instead of treating the problem in approximate form, *viz.* using an estimate of this mean equivalent width as done is most of the litterature on transmissivity based models, the problem is studied here in its general form. This requirement is related to the ℓ-distribution formulation. The second one is based on the observation that as soon as an idea of path reordering is considered, the transmissivity of any non-uniform path involving the same set of absorption coefficients $\kappa_i, i = 1, .., n$ needs to be represented by the same ordering of the indices $i = 1, .., n$. In some configurations, the emission point will be associated with index 1, in others with index 2, *etc.* This means that in reordered models, it is not sufficient to consider inequalities of

the type of Eq. (25) at the last point encountered along the radiation path, but all possible configurations must be considered at once. This is why we have formulated the problem in terms of the system of inequalities Eq. (25) and not as:

$$-\frac{\partial \tau_{1..j}^{\Delta\nu}(L_1,..,L_j)}{\partial L_j} \leq k_P^j \; \tau_{1..j}^{\Delta\nu}(L_1,..,L_j), j = 1,..,n \tag{26}$$

which is the more usual formulation obtained by considering the propagation of radiation emitted at the j-th location along the path up to the layer with index 1. The main difference between the two systems of inequalities is that in the set Eq. (26) only transmissivities up to an index j are considered (all indices higher than $j+1$ are skipped) whereas in the set Eq. (25), all indices up to the highest possible one, n, are treated simultaneously. Notice that if Eq. (25) is correct then Eq. (26) is valid too: this is due to the fact that Eq. (26) can be written as a particular case of Eq. (25) for which $L_{j+1} = 0,..,L_n = 0$. However, the reciprocal may be wrong in the general frame.

In the GWN method, the non-uniform transmissivity $\tau_{1..n}^{\Delta\nu}(L_1,..,L_n)$ is modeled as the transmissivity of the gas in state 1 with an equivalent length $L_{1..n}$, *viz.* $\tau_{1..n}^{\Delta\nu}(L_1,..,L_n) = \tau_1^{\Delta\nu}(L_{1..n})$ where the length $L_{1..n}$ is defined recursively as:

$$L_{nn} = L_n \tag{27}$$

$$L_{i..n} = L_i + \ell_i \circ \tau_{i+1}^{\Delta\nu}(L_{i+1..n}), i = 1,..,n-1 \tag{28}$$

The previous equation can be also written in terms of effective scaling factors, as defined in the previous section, as:

$$L_{i..n} = L_i + u(L_{i+1..n})L_{i+1..n}, i = 1,..,n-1 \tag{29}$$

This process is equivalent to the recursive definition of function $\mathcal{C}_{1..n}$ as:

$$\mathcal{C}_{nn}(X_n, 1) = X_n \tag{30}$$

$$\mathcal{C}_{i..n}(X_i,..,X_n) = \mathcal{C}_{ii}\left[X_i, \mathcal{C}_{i+1,..,n}\left(X_{i+1},..,X_n\right)\right], i = 1,..,n-1 \tag{31}$$

For our model to be physically realistic, we may impose the transmissivity $\tau_1^{\Delta\nu}(L_{1..n})$ to follow the inequalities observed for the true non-uniform path

transmissivities, *i.e*, Eqs. 25. In the following, only the cases of two and three cells are treated. The more general case follows the same steps and its treatment is not informative, but is more tedious.

Our objective is thus to find in which condition on the choice of indices $1, 2$ the following inequalities are simultaneously verified:

$$-\frac{\partial \tau_1^{\Delta\nu}(L_{12})}{\partial L_1} \leq k_P^1 \, \tau_1^{\Delta\nu}(L_{12}) \tag{32}$$

$$-\frac{\partial \tau_1^{\Delta\nu}(L_{12})}{\partial L_2} \leq k_P^2 \, \tau_1^{\Delta\nu}(L_{12}) \tag{33}$$

The first inequality is always verified, as a direct application of Chebyshev inequality for integrals and using the fact that κ_ν and $exp\left(-\kappa_\nu L_{1..n}\right)$ have opposite monotonicity with respect to wavenumber ν, *i.e.*:

$$-\frac{\partial \tau_1^{\Delta\nu}(L_{12})}{\partial L_1} = \frac{1}{\Delta\nu}\int_{\Delta\nu} \kappa_\nu^1 exp\left(-\kappa_\nu^1 L_{1..n}\right) d\nu \leq \underbrace{\frac{1}{\Delta\nu}\int_{\Delta\nu} \kappa_\nu^1 d\nu}_{k_P^1} \times \underbrace{\frac{1}{\Delta\nu}\int_{\Delta\nu} exp\left(-\kappa_\nu^1 L_{1..n}\right) d\nu}_{\tau_1^{\Delta\nu}(L_{1..n})} \tag{34}$$

The second inequality mostly follows the same steps. Indeed:

$$\frac{\partial \tau_1^{\Delta\nu}(L_{12})}{\partial L_2} = \frac{\partial \tau_1^{\Delta\nu}(L_{12})}{\partial L_{12}}\frac{\partial L_{12}}{\partial L_2} = \frac{\partial \tau_1^{\Delta\nu}(L_{12})}{\partial L_{12}}\frac{\partial \ell_1 \circ \tau_2^{\Delta\nu}(L_2)}{\partial L_2} \tag{35}$$

Application of Chebyshev inequality to the first derivatives at the RHS then provides:

$$-\frac{\partial \tau_1^{\Delta\nu}(L_{12})}{\partial L_2} \leq k_P^1 \, \tau_1^{\Delta\nu}(L_{12})\frac{\partial \ell_1 \circ \tau_2^{\Delta\nu}(L_2)}{\partial L_2} \tag{36}$$

It follows that a sufficient condition for Eqs. (25) and (36) to coincide is:

$$\frac{\partial \ell_1 \circ \tau_2^{\Delta\nu}(L_2)}{\partial L_2} \leq \frac{k_P^2}{k_P^1} = \frac{\partial \ell_1 \circ \tau_2^{\Delta\nu}(L_2 = 0)}{\partial L_2} \tag{37}$$

The second equality arises directly from the definition of function $\ell_1 \circ \tau_2^{\Delta\nu}(L_2)$. Consequently, it is sufficient that $\ell_1 \circ \tau_2^{\Delta\nu}(L_2)$ is concave (its second derivative with respect to L_2 is in this case negative and thus $\frac{\partial \ell_1 \circ \tau_2^{\Delta\nu}(L_2)}{\partial L_2}$ decreases and

is lower than its value in $L_2 = 0$) to ensure that the system of inequalities Eqs. (32,33) is actually verified. The case of three layers (and more generally of n uniform layers, by induction) follows the same steps for $i = 1, 2$. Only the case of the third layer differs and is detailed below.

The derivative of the transmissivity of the non-uniform path with respect to the length of the third path is given as:

$$\frac{\partial \tau_1^{\Delta\nu}(L_{123})}{\partial L_3} = \frac{\partial \tau_1^{\Delta\nu}(L_{123})}{\partial L_{123}} \frac{\partial L_{123}}{\partial L_3} = \frac{\partial \tau_1^{\Delta\nu}(L_{123})}{\partial L_{123}} \frac{\partial \ell_1 \circ \tau_2^{\Delta\nu}(L_{23})}{\partial L_3} \tag{38}$$

which is the same as Eq. (35). However, following the definition of L_{23} as $L_{23} = L_2 + \ell_2 \circ \tau_3^{\Delta\nu}(L_3)$ one has (by application of the chain rule):

$$\frac{\partial \ell_1 \circ \tau_2^{\Delta\nu}(L_{23})}{\partial L_3} = \frac{\partial \ell_1 \circ \tau_2^{\Delta\nu}(L_{23})}{\partial L_{23}} \frac{\partial L_{23}}{\partial L_3} = \frac{\partial \ell_1 \circ \tau_2^{\Delta\nu}(L_{23})}{\partial L_{23}} \frac{\partial \ell_2 \circ \tau_3^{\Delta\nu}(L_3)}{\partial L_3} \tag{39}$$

Once reported inside Eq. (36), one then obtains:

$$-\frac{\partial \tau_1^{\Delta\nu}(L_{123})}{\partial L_3} \leq k_P^1 \, \tau_1^{\Delta\nu}(L_{123}) \frac{\partial \ell_1 \circ \tau_2^{\Delta\nu}(L_{23})}{\partial L_{23}} \frac{\partial \ell_2 \circ \tau_3^{\Delta\nu}(L_3)}{\partial L_3} \tag{40}$$

A sufficient condition for this inequality to follow Eq. (25) with $i = 3$, and assuming that levels 1 and 2 are organized in such a way that inequality Eq. (37) is actually verified, in which case $\frac{\partial \ell_1 \circ \tau_2^{\Delta\nu}(L_{23})}{\partial L_{23}} \leq \frac{k_P^2}{k_P^1}$, is:

$$\frac{\partial \ell_2 \circ \tau_3^{\Delta\nu}(L_3)}{\partial L_3} \leq \frac{k_P^3}{k_P^2} = \frac{\partial \ell_2 \circ \tau_3^{\Delta\nu}(L_3 = 0)}{\partial L_3} \tag{41}$$

This follows directly from the fact that if the layers are organized this way, we have:

$$-\frac{\partial \tau_1^{\Delta\nu}(L_{123})}{\partial L_3} \leq k_P^1 \, \tau_1^{\Delta\nu}(L_{123}) \, \frac{k_P^2}{k_P^1} \, \frac{k_P^3}{k_P^2} = k_P^3 \, \tau_1^{\Delta\nu}(L_{123}) \tag{42}$$

The problem of path reordering can thus be reformulated in the following terms:

$$\text{find a permutation } \sigma : \{1,..,n\} \to \{1,..,n\} \text{ such that: } \frac{\partial^2 \ell_{\sigma(i)} \circ \tau_{\sigma(i+1)}^{\Delta\nu}(L)}{\partial L^2} \leq 0 \tag{43}$$

This problem can benefit from results from copulas theory, as explained in the next section.

3.3. Useful mathematical results

As emphasized previously, the GWN method can be naturaly formulated in terms of Archimedean copulas. It is out of the scope of the present paper to provide a full description of this mathematical framework, but only to use some elements of this theory, useful for the purpose of obtaining a reorganization of the gaseous layers in such a way that the constraints provided in the previous section are actually verified or can be at least considered as such. More details on copulas can be found for instance in Ref. [19, 21].

Following Archimedean copula's theory, the structure determination of hierarchical (or nested) Archimedean copulas (HAC) can be made by analysis of Kendall's $\mathcal{K}e$ correlation coefficient [22, 23]. In the case of a bivariate Archimedean copula associated with a twice differentiable generator ϕ with $\phi > 0$ for all $t \in [0, +\infty)$, this coefficient is defined as [22]:

$$\mathcal{K}e(\phi) = 1 - 4 \int_0^{+\infty} t \left[\phi'(t)\right]^2 dt \tag{44}$$

which provides, all calculations done with $\phi = \tau^{\Delta\nu}$, *i.e.*, $t \leftarrow L$ and $\phi' \leftarrow \frac{\partial \tau^{\Delta\nu}(L)}{\partial L}$:

$$\mathcal{K}e(\tau^{\Delta\nu}) = \frac{1}{\Delta\nu^2} \int_{\Delta\nu} \int_{\Delta\nu} \left(\frac{\kappa_\nu - \kappa_{\nu'}}{\kappa_\nu + \kappa_{\nu'}} \right)^2 d\nu \, d\nu' \tag{45}$$

From this formula, it is obvious that two scaled spectra share the same value of Kendall's coefficient.

Kendall's coefficient is a so-called mesure of concordance [19, 21]. It can be shown (see Appendix A for details) that given two transmissivity curves $\tau_1^{\Delta\nu}$ and $\tau_2^{\Delta\nu}$:

$$\mathcal{K}e(\tau_1^{\Delta\nu}) \geq \mathcal{K}e(\tau_2^{\Delta\nu}) \Rightarrow \text{one can find } L \geq 0 \text{ such that} \frac{\partial^2 \ell_2 \circ \tau_1^{\Delta\nu}(L)}{\partial L^2} > 0 \quad (46)$$

The analysis of Kendall's coefficient thus allows determining the "wrong" direction and thus its opposite can be used as the "good" one. However, it should be noticed that the ordering of the layers in terms of the Kendall's coefficients does not ensure that Eq. (43) is actually verified because the two sides of Eq. (46) are not rigorously equivalent. But from the analysis of Kendall's coefficient, we can however find one direction for which it is sure that our constraint is not verified and thus choose the opposite direction to construct our iterative scheme.

The physical meaning of Kendall's coefficient can be explored further by considering two spectra, κ_ν^1 and κ_ν^2 made of the same spectral lines with distinct profiles and linestrengths and such that, for instance, $\mathcal{K}e(\tau_2^{\Delta\nu}) > \mathcal{K}e(\tau_1^{\Delta\nu})$. We can construct a third absorption spectrum by $\kappa_\nu^3 = \frac{k_P^1}{k_P^2}\kappa_\nu^2$. As κ_ν^2 and κ_ν^3 are scaled by definition, they share the same Kendall's coefficient, *viz.*, $\mathcal{K}e(\tau_2^{\Delta\nu}) = \mathcal{K}e(\tau_3^{\Delta\nu})$. Combining this equality with $\mathcal{K}e(\tau_2^{\Delta\nu}) > \mathcal{K}e(\tau_1^{\Delta\nu})$, we obtain that $\mathcal{K}e(\tau_3^{\Delta\nu}) > \mathcal{K}e(\tau_1^{\Delta\nu})$. The derivative with respect to the length L of the band averaged transmissivities for the spectra κ_ν^1 and κ_ν^3 are the same at the optically thin limit (they are equal to the Planck mean absorption coefficients which are obviously the same for these spectra) but, following the previous inequality, are associated with distinct values of Kendall's coefficients. This means that values of Kendall's coefficients are more affected by the wings of the spectral lines than by their centers. This idea can be explored further in the case of the SNB-LM model, for which the transmissivity of a gas path of total length L is given as:

$$\tau^{SNB-LM}(L) = \exp\left[-\frac{\beta}{\pi}\left(\sqrt{1+\frac{2\pi k_P L}{\beta}}-1\right)\right] \quad (47)$$

where k_P is the mean absorption coefficient (Planck mean) over the band and β characterizes the overlapping between spectral lines. The corresponding Kendall's coefficient $\mathcal{K}e$ is:

$$\mathcal{K}e(\tau^{SNB-LM}) = \frac{1}{2} + \frac{2\beta^2}{\pi^2} exp\left(\frac{2\beta}{\pi}\right) Ei\left(\frac{2\beta}{\pi}\right) - \frac{\beta}{\pi} \tag{48}$$

where Ei represents the Exponential integral:

$$Ei(p) = \int_1^{+\infty} \frac{\exp(-px)}{x} dx \tag{49}$$

As noticed in Eq. (48), in the case of the SNB-LM, the Kendall's coefficient only depends on the overlapping parameter β. This result is in accordance with our previous analysis on the physical interpretation of this coefficient as a characteristic of line wings. Function $\mathcal{K}e(\tau^{SNB})$ is depicted as a function of the overlapping parameter β in Figure 2. Its maximum value is $\frac{1}{2}$ when $\beta \to 0$ and admits the limit 0 when the gas spectrum is gray, i.e., $\kappa_\nu = constant$. $\mathcal{K}e(\tau^{SNB})$ decreases with respect to the parameter β.

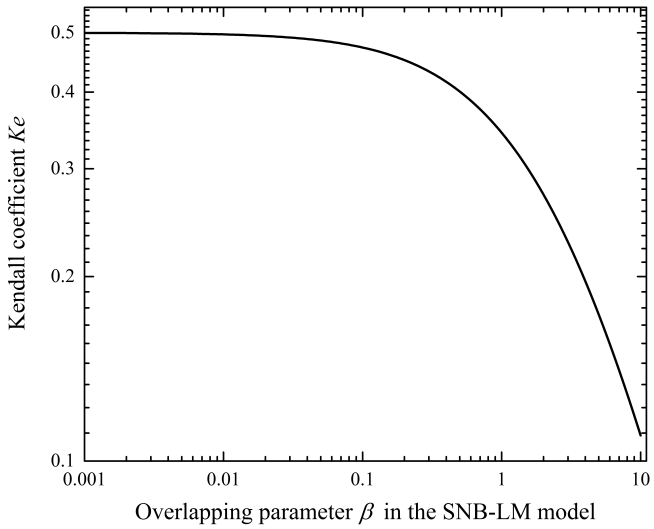

Figure 2: Kendall coefficient as a function of overlapping parameter β

For two thermophysical states for which the gas spectra follow rigorously the assumptions of the SNB-LM, it was shown in Ref. [9] that:

$$\ell_1 \circ \tau_2^{\Delta\nu}(L_2) = \frac{k_P^2\beta_2}{k_P^1\beta_1}L_2 + \frac{k_P^2}{k_P^1}\left(1-\frac{\beta_2}{\beta_1}\right)\frac{\beta_2}{\pi k_P^2}\left(\sqrt{1+\frac{2\pi k_P^2 L_2}{\beta_2}}-1\right) \quad (50)$$

$$= \frac{k_P^2\beta_2}{k_P^1\beta_1}L_2 + \int_0^{+\infty} f(s)\left[1-\exp(-sL_2)\right]ds$$

where:

$$f(s) = \frac{1}{\sqrt{2\pi}}\left(\frac{\beta_2}{\pi k_P^2}\right)^{\frac{1}{2}}\frac{k_P^2}{k_P^1}\left(1-\frac{\beta_2}{\beta_1}\right)s^{-\frac{3}{2}}\exp\left(-\frac{\beta_2 s}{2\pi k_P^2}\right) \quad (51)$$

From Eqs. (48) and (50), one can observe that a decrease in the $\mathcal{K}e$ coefficient is associated with an increase of the overlapping parameter β. In this case of increasing β parameter (from cell 2 to cell 1, viz. $\beta_1 \geq \beta_2$), Eq. (50) shows that function $\ell_1 \circ \tau_2^{\Delta\nu}(L_2)$ is then concave (its second derivative with respect to L_2 is in this case negative). A calculation made in the direction of decreasing $\mathcal{K}e$ provides in this situation a so-called Levy-subordinated Archimedean copula [24, 9] (this name is related to the fact that $\ell_1 \circ \tau_2^{\Delta\nu}(L_2)$ is then a Bernstein function, *i.e.*, its derivative is a Laplace transform, as shown in Eqs. (50,51), more usually called in the context of statistical studies, a Laplace exponent of a Levy subordinator [25]).

4. Application and results

In this section, the accuracy and computational cost of the ℓ-distribution method based on two reordering schemes is assessed against LBL calculations. The first reordering scheme, called β reordering, uses the set of indices of the various atmospheric layers obtained by a reordering of the layers with respect to decreasing values of the parameter β as defined by Eq. (5). It thus corresponds to the reordering scheme introduced in Ref. [9] and mostly consists of neglecting the effect of the mapping functions Gr since this path ordering strategy is the same as that of the germ models. The second reordering scheme, called $\mathcal{K}e$ reordering, uses a reordering of the gas path with respect to decreasing values of the Kendall coefficient defined by Eq. (44). This second reordering scheme

thus accounts for possible effects of the Gr functions. It can be noticed here that both reordering schemes suggest a treatment of the gaseous layers from the top of the atmosphere down to the ground. The only difference is that in the case of a reordering with respect to the $\mathcal{K}e$ coefficient, the 11th layer starting from the ground needs to be placed after all other layers. Physical reasons that could explain this result have not been found yet. However, following the analysis provided in Ref.[16] this result suggests that the spectral content of full paths for the TOA down to the ground is closer (more linearly scaled) with the spectrum at the 11th layer in the atmosphere than that close to the ground surface. Results of a Correlated k-distribution (Ck) [4] model with various number of gray gases based on Gauss-Legendre quadratures at orders from 16 up to 256 are also provided for completeness. For the ℓ-distribution method, high resolution mapping functions made of 50,000 values were used. This large number of values has no influence on the calculation cost of the technique but requires more memory space for the application of the method. Using high resolution mapping functions allows focusing on the effect of the reordering scheme only, which is the main aim of the present work.

Two types of conditions are studied. The first one considers clear sky non-scattering situations, for which transmissivities of non-uniform paths are compared (this is the situation for which a perfect miror is put at some given altitude). The second type of comparison involves scattering events (molecular and/or by clouds). This more realistic situation was treated by incorporating the ℓ-distribution model inside the atmospheric code 3DMCPOL [26] based on a Monte Carlo RTE solver, developed at the Laboratory of Atmospheric Optics in Lille, France. All calculations were made under the standard Mid-Latitude Summer (MLS) atmospheric profile [11]. The transmission in the A-band of oxygen and the filter response function used in this study are shown in Figure 3 in the case of an Air Mass Factor of 1 (one single Nadir path in the atmosphere). This spectral response is characteristic of instruments that use the A-band of oxygen, with measurements both in the O_2 absorption and outside the absorption band or with a weak O_2 absorption (such as MERIS [27], POLDER [28]

or the future instrument 3MI [29]). The O_2 A-band is widely used in remote sensing (see [30, 31, 32] and references therein) for the determination of the atmospheric pressure near the ground or above clouds, as well as for the determination of the altitude at which scattering aerosols can be found. The LBL code used for the high resolution calculations is described in [33].

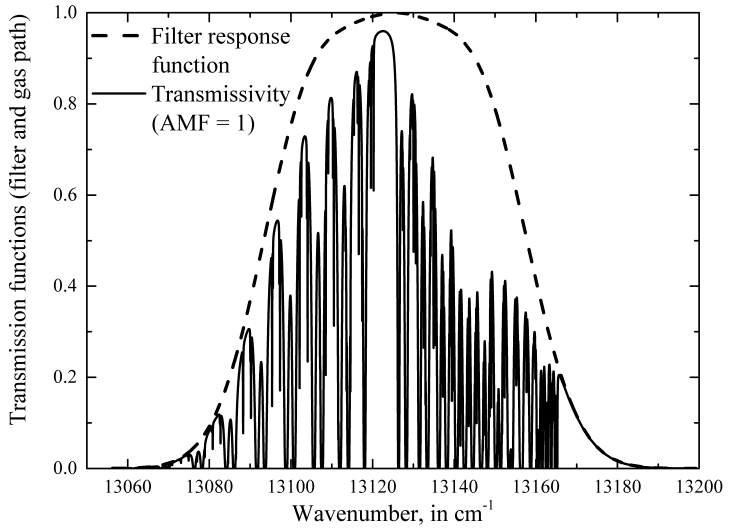

Figure 3: Filter response function and gas path transmissivity accounting for the filter response for AMF=1

Results, assuming a surface albedo of 0.2 fixed in all simulations involving scattering events, are provided in terms of the Air Mass Factor (AMF) defined as:

$$\mathrm{AMF} = \frac{1}{\cos(\theta_0)} + \frac{1}{\cos(\theta_v)} \tag{52}$$

where θ_0 and θ_v are the solar and satellite viewing angles respectively. Relationships between values of AMF used in the various figures and the corresponding couples of angles θ_0 and θ_v are given in Table 1.

AMF	θ_0	θ_v
2	0	0
4	60	60
16	84.4	80

Table 1: Relationship between viewing angles, in degrees, and Air Mass Factor (AMF) - viewing azimuth angle is 180 degrees from the sun azimuth in the specular direction

4.1. Clear sky non-scattering conditions

These cases are mostly used to evaluate the accuracy of the various approximate methods in situations of pure gaseous absorption. Results are depicted in Figures 4 to 6. In these figures, the accuracy of both ℓ-distribution methods is found higher than the Ck model with 256 gray gases. It was observed, but the results are out of the scope of the present work, that this Ck method provides the same results as a true correlated LBL model obtained by associating at the spectral scale values of absorption coefficient inside different layers through the same relationship, based on equality of the corresponding cumulative distribution functions, as the gray gases Ck model. Results of this technique can thus be considered as the limit in terms of accuracy of a model based on the so-called correlation assumption for this specific problem (O_2 A-band in the MLS configuration).

The largest relative errors for the ℓ-distribution method are below 0.8 % in all the cases considered. The mean value of relative errors evaluated over the full range of pathlengths considered in the case of Figure 6 (240 values) is 10.2 10^{-4} for Ck vs LBL whereas it is 7.54 10^{-4} /beta (7.4766 10^{-4} / Kendall) for ℓ-distribution vs LBL. This means that at a global scale the ℓ-distribution method is more accurate than the correlated k-distribution. However, the ℓ-distribution method provides in some cases (for some values of pathlengths) results less accurate than correlated k-distributions.The effect of β vs $\mathcal{K}e$ reordering scheme is noticeable in the lower layers of the atmosphere, where the orders of the paths are different. Nevertheless, the $\mathcal{K}e$ reordering scheme is found to provide slightly

more accurate estimates of the transmissivities of the non-uniform paths than the β reodering scheme in all the cases treated. The two methods share in this case the same computational cost as only the orders of treatment of the set of lenghts $L_1, ...L_n$ differs between the two calculations.

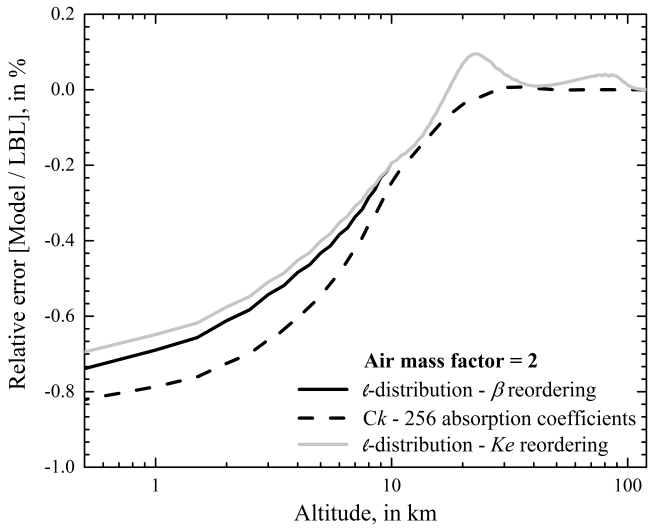

Figure 4: Non-uniform transmission curves for AMF=2

4.2. Scattering conditions - case of cloudy atmospheres

All calculations in the following scattering situations were made with the code 3DMCPOL. This Monte Carlo radiative transfer simulator was compared recently to several other atmospheric codes in Refs. ([34], [35]).

These cases treat radiative transfer in the atmosphere considering scattering events. They were simulated by separating the treatment of scattering from molecular absorption. The method used in combination with the ℓ-distribution approach is the following: 1/ a photon is launched from space and propagates in the atmosphere until a first scattering event occurs, 2/ one part of the radiative energy associated with the photon is sent to the imaging device, including the

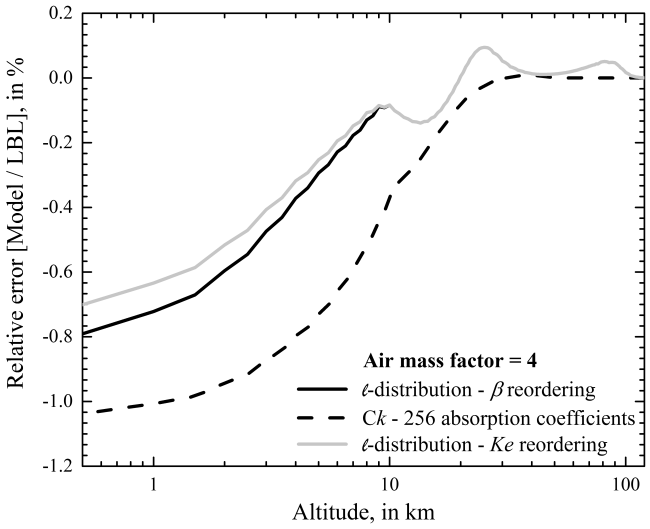

Figure 5: Non-uniform transmission curves for AMF=4

contribution of gaseous absorption between the location of the scattering event and the sensor, 3/ the total lengths of the gas paths in the various atmospheric layers seen by the photon are calculated, 4/ the transmissivity of the non-uniform gas path is then evaluated, 5/ the energy of the photon that reaches the detector is multiplied by this transmissivity to account for molecular absorption and the radiative energy measured by the detector is updated, 6/ a new direction and propagation length are chosen at the point of the scattering events and the process is iterated (back to step 2) until the remaining energy of the photon reaches some cut-off or leaves the atmosphere. This method is applied to a significant amount of (10^6) photon paths in order to provide a proper statistical estimate of the simulated radiance.

4.2.1. Pure Molecular Scattering

The first scattering configuration only involves molecular scattering (Rayleigh). Results are depicted in Figures 7 (calculation cost) and 8 (accuracy). In these

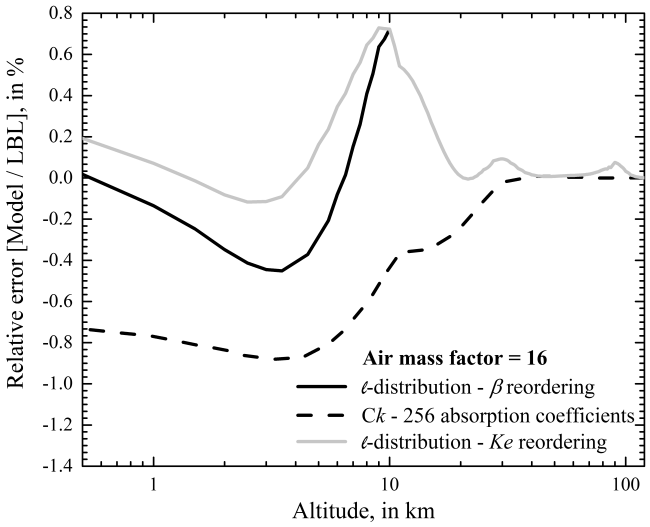

Figure 6: Non-uniform transmission curves for AMF=16

cases, both ℓ-distribution methods (β and $\mathcal{K}e$ reordering schemes) provide the highest improvements in terms of computational cost (higher than 1,000) compared to LBL calculations. On the same cases, the CPU time ratio for the Ck model with 16 coefficients remains lower than 800. Furthermore, the ℓ-distribution models based on the $\mathcal{K}e$ reordering scheme appears to be the most accurate, confirming the results provided in the previous section (cases without scattering).

4.2.2. Scattering by clouds – mono- and multi-layers

O_2 A-Band information is widely used to retrieve cloud [36, 37] and aerosol [38] geometrical properties. The second series of tests was consequently made in cloudy atmosphere composed of uniform layers with cloud droplet size distribution of effective radius of 10μm. As cloud are optically dense media, scattering processes are numerous and the photons path lengths can be high in the cloud layers. In order to evaluate this effects on the ℓ-distribution method at different

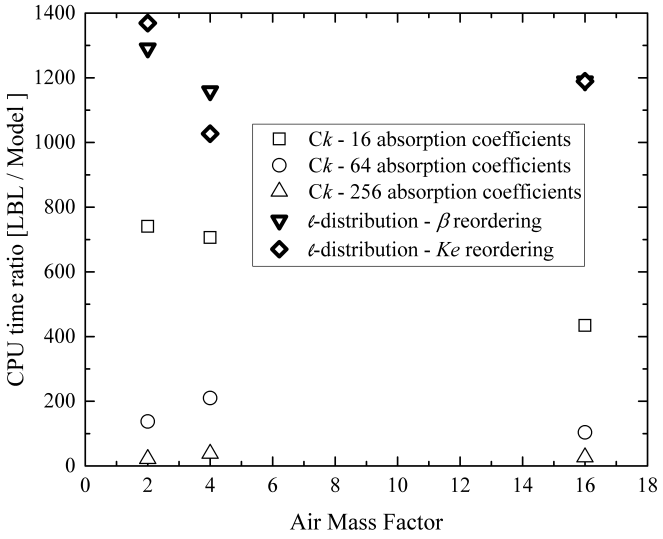

Figure 7: Gain in terms of CPU time - RTE solver: 3DMCPOL Monte Carlo code - Pure molecular Scattering

levels, two mono-layer clouds were considered : the first one, typical of a stratocumulus cloud, has an optical thickness of 10 and is located between 1 and 2 km (Figures 9 and 10); the second one, representative of a semi-transparent high cloud, has an optical thickness of 2 and is located between 10 and 11 km (Figures 11 and 12).

Figures 10 and 12 show that, as previously, the computation cost is reduced significantly with the ℓ-distribution method in comparison with the LBL and Ck methods. The computation time is decreased by a factor comprised between 500 and 1000 compared to the reference LBL calculation. It corresponds to a gain of about 14 to 84 % compared to k-distribution computation with 16 coefficients. In addition, the accuracy is higher for ℓ-distribution and in particular for the Kendall reordering in the low cloud case (Figure 9). For the high cloud case, the accuracy of the ℓ-distribution method is in most cases, higher than the

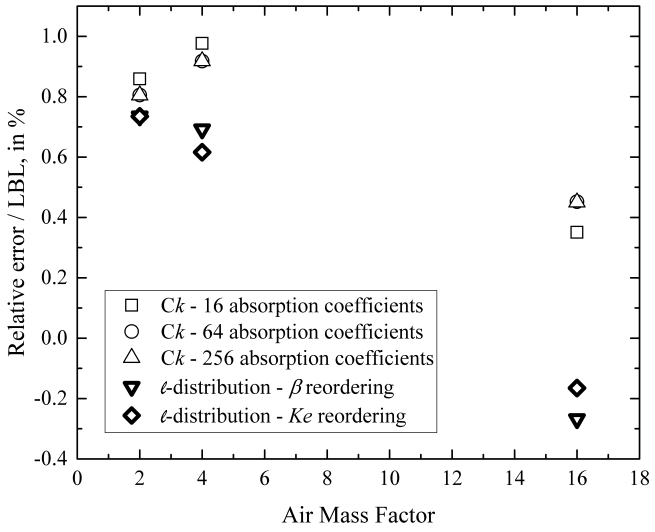

Figure 8: Relative Error / LBL - Pure molecular Scattering

k-distribution, except for the largest airmass factor of 16.

Finally, ℓ-distribution was applied to a multi-layer cloud made of the two mono-layer situations studied previously. In this case, the reflections between the two clouds increase the lengths of the path of the photons in the most absorbing parts of the atmosphere. This configuration is thus a complete test for the ℓ-distribution method. Results, depicted in Figure 13, show again a better accuracy than the k-distribution for the airmass factors of 2 and 4 but, driven certainly by the high cloud results, the accuracy is lower for the airmass factor of 16. However, as for other cases, the computation cost is reduced by 30% for the airmass factor 2 and about 60% for the airmass factors 4 and 16, as shown in figure 14.

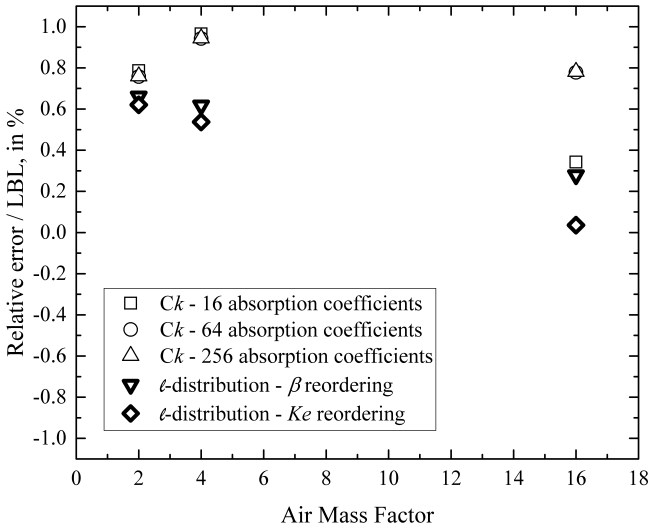

Figure 9: Relative Error / LBL - cloud between 1 and 2 km with COT = 10

5. Summary and conclusion

A method to estimate the radiative properties of non-uniform gaseous paths was described. It uses a combination of tabulated transmissivities of uniform paths and a non-uniform approximation based on the definition of effective scaling factors. The uniform model allows a fast and accurate handling of the implicit equation used to define these effective scaling factors. This non-uniform approximation (GWN) is found to be closely related to the theory of Hierarchical Archimedean copulas. This allows using directly elements from this theory to propose a reorganization of the paths in such a way that some physical constraints, discussed in the paper, are actually verified.

Once reordered, it is shown that the method is capable of reproducing mean radiance calculated LBL with an accuracy higher than 1% at a tiny fraction of the computational cost of a high resolution model (up to 1,000), both in clear sky and cloudy simulations. In addition, it is shown that the present ℓ-

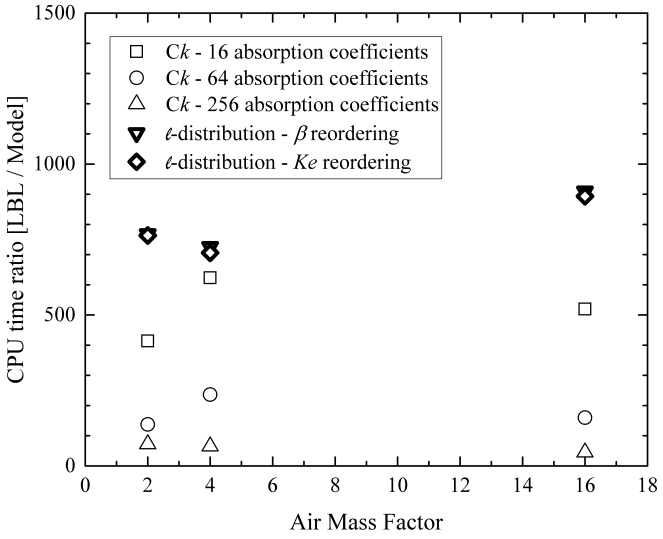

Figure 10: Gain in terms of CPU time - RTE solver: 3DMCPOL Monte Carlo code - cloud between 1 and 2 km with COT = 10

distribution method can compete and in some cases outperform the more usual Ck approach both in terms of accuracy and computational cost.

The main defect of the present technique is its formulation in transmission form which restricts its application to methods based on the integral formulation of the RTE such as ray-tracing, but do not allow its use together with a discrete ordinate [39], Matrix operator or adding-doubling solver of the RTE, for instance. However, due to its high efficiency, the technique can be a good candidate for applications that can accomodate with such a formulation, including Monte-Carlo (as used here) or quasi-Monte Carlo methods. For these kinds of RTE solvers, the ℓ-distribution approach can provide accurate results at small computational cost and thus find applications in near real time sensing problems.

It should be noticed that the present paper only focuses on the application of the ℓ-distribution approach in the visible range. Evaluations of the technique

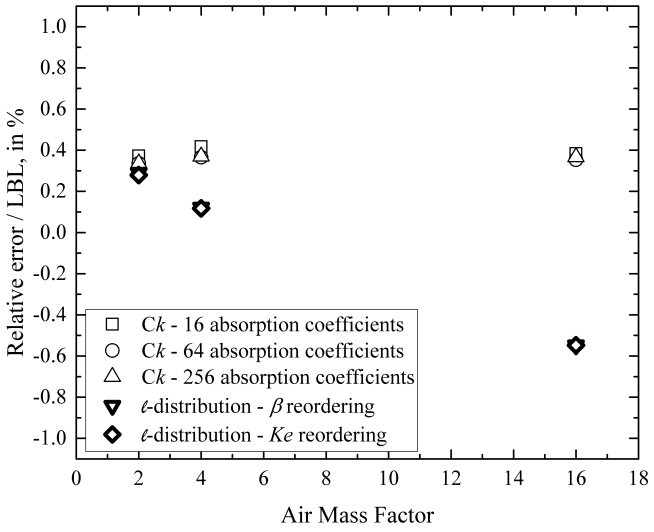

Figure 11: Relative Error / LBL - cloud between 10 and 11 km with COT = 2

in the thermal infrared region has always been conducted in high temperature applications and found to provide more accurate results than the Ck method for the treatment of gas mixtures: applications of the method for thermal infrared radiative transfer in the atmosphere are scheduled as a continuation of the present work. The work presented here is for moderate resolution imagers. A preliminary study shows that the developed method works for high resolution spectrometers, such as IASI-NG, too: high resolution calculations will be explored further and these preliminary results will be confirmed in future works.

Appendix A. Theoretical justification of relationship (46)

The aim of this appendix is to provide a justification of the relationship (46). It is based on the following definitions and theorems taken from Nelsen [19]. The notation $<_c$ represents the concordance ordering, *i.e.*, $\mathcal{C}_1 <_c \mathcal{C}_2$ if $\mathcal{C}_1(x, y) \leq \mathcal{C}_2(x, y)$ for any couple x, y inside the unit square. The concept of

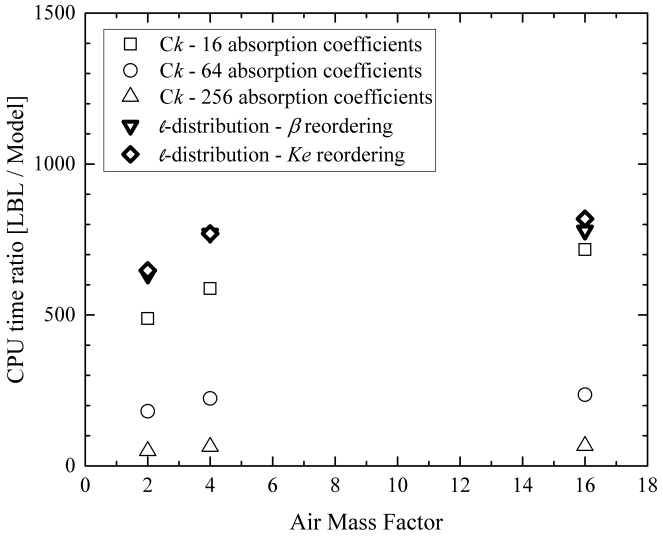

Figure 12: Gain in terms of CPU time - RTE solver: 3DMCPOL Monte Carlo code - cloud between 10 and 11 km with COT = 2

concordance between random variables is fundamental in copula's theory.

In the following, Ω represents the set of continuous strictly decreasing convex functions ϕ from [0,1] to $[0,+\infty)$ with $\phi(1) = 0$. Obviously, inverse functions ℓ of band averaged transmissivities (including possible effects of filter functions) are elements of Ω. The convexity property of ℓ arises directly from the convexity property of transmission functions (their second derivative with respect to the gas path lengths are positive) combined with the fact that ℓ is decreasing from $+\infty$ for null values of transmissivities down to 0 when transmissivities are equal to 1.

Definition 1. *A measure of association μ between two continuous random variables X and Y whose copula is $\mathcal{C}$ is a measure of concordance if it satisfies the following properties:*

1. *μ is defined for every pair of random variables*

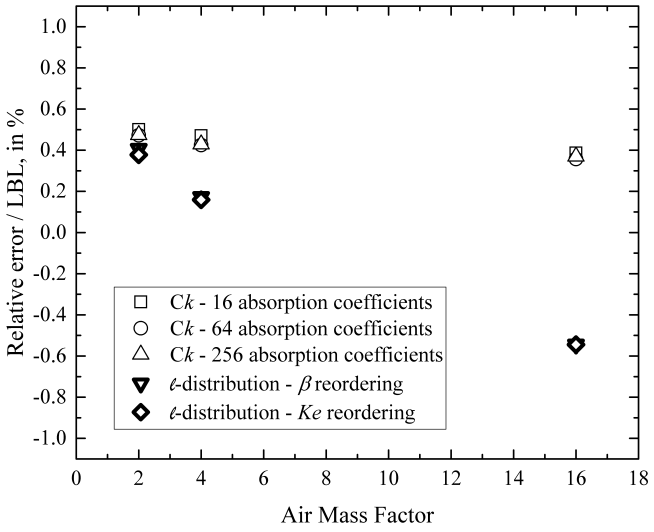

Figure 13: Relative Error / LBL - double layer of clouds between 1 and 2 km with COT = 10 and between 10 and 11 km with COT = 2

2. *-1* $\leq \mu \leq$ *1*

3. $\mu_{X,Y} = \mu_{Y,X}$

4. *if* X *and* Y *are independent, then* $\mu_{\mathcal{C}} = \mu_{X,Y} = 0$

5. *if* $\mathcal{C}_1$ *and* $\mathcal{C}_2$ *are copulas such that* $\mathcal{C}_1 <_c \mathcal{C}_2$ *then* $\mu_{\mathcal{C}_1} \leq \mu_{\mathcal{C}_2}$

Kendall's coefficients as defined by Eq.(44) are measures of concordance. A proof can be found for instance in Nelsen [19]. The following theorem can be also found on the same reference.

Theorem 1. *Let* $\mathcal{C}_1$ *and* $\mathcal{C}_2$ *be Archimedean copulas generated respectively by* ℓ_1 *(inverse of* $\tau_1^{\Delta\nu}$*) and* ℓ_2 *(inverse of* $\tau_2^{\Delta\nu}$*) in* Ω*. If* $\ell_1 \circ \tau_2^{\Delta\nu}$ *is concave then* $\mathcal{C}_1 <_c \mathcal{C}_2$*.*

Accordingly, the combination of theorem 1 with property 5. from the definition of measures of concordance shows that if $\ell_1 \circ \tau_2^{\Delta\nu}$ is concave then $\mathcal{K}e_1 \leq \mathcal{K}e_2$

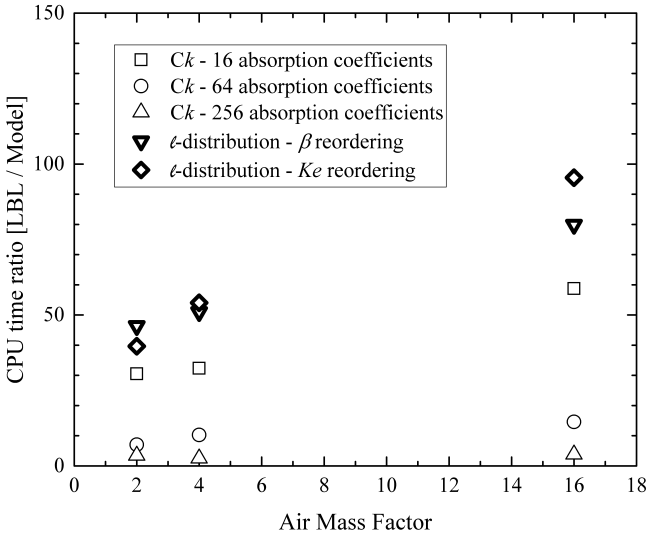

Figure 14: Gain in terms of CPU time - RTE solver: 3DMCPOL Monte Carlo code - double layer of clouds between 1 and 2 km with COT = 10 and between 10 and 11 km with COT = 2

or, equivalently, if $\mathcal{K}e_1 > \mathcal{K}e_2$ then one can find a value L_2 such that $\frac{\partial \ell_1 \circ \tau_2^{\Delta\nu}(L_2)}{\partial L_2}$ increases. Consequently, the analysis of $\mathcal{K}e$ coefficients allows finding a direction for which the derivative of function $\ell_1 \circ \tau_2^{\Delta\nu}$ is not decreasing. The other direction can then be used as the "good one" for the calculations. In the case of gas spectra that follow rigorously the assumptions of the SNB-LM model, this choice of decreasing Kendall's coefficients was shown in the paper to ensure the concavity of the corresponding $\ell_1 \circ \tau_2^{\Delta\nu}$ function (see Eqs. (48) and (50)). This result is typical of one parameter copula families as generated by SNB-LB models which yield copulas that depend on a single parameter (the β coefficient in the present case). It is generalized here but the principle is founded on the same kind of mathematical analysis.

Appendix B. Nomenclature and list of acronyms

Latin symbols

$\mathcal{C}$	Copula
Gr	mapping function
$\mathcal{K}e$	Kendall's coefficient
ℓ	inverse of the transmission function
L	gas path length
T	temperature of the gas layer, in K
u	scaling coefficient related to ratio of gas spectra
X, Y	dummy variables, between 0 and 1

Greek symbols

β	overlapping parameter
δL	small path increment, in cm
$\Delta\nu$	width of the spectral band , in cm^{-1}
κ_ν	spectral absorption coefficient, in cm^{-1}
Λ	inverse of the germ transmission function
$\phi(\nu)$	filter response function
$\phi(t)$	generator of an Archimedean copula
Φ	integral of the filter response function over the band $\Delta\nu$
ν	wavenumber, in cm^{-1}
τ	transmission function, transmissivity

Subscripts and superscripts

P	Planck mean
R	Rosseland mean
0	related to the germ model
$1, 2, .., n$	related to the first, second,.. uniform gaseous path
$1..n$	related to the non-uniform path made of subpaths from 1 to n

Acronyms

4A/OP	Automatized Atmospheric Absorption Atlas
RTE	Radiative Transfer Equation
Ck	Correlated k-distribution method
GWN	Godson-Weinreb-Neuendorffer's method
SNB-LM	Statistical Narrow Band model (Lorentz lines, Makmus' distribution of linestrengths)

Acknowledgments

This work has been supported by the Programme National de Télédétection Spatiale (PNTS, http://www.insu.cnrs.fr/pnts grant PNTS-2017-04).

References

[1] S. Clough, M. J. Iacono, J.-L. Moncet, Line-by-line calculation of atmospheric fluxes and cooling rates: Application to water vapor, Journal of Geophysical Research 97 (1992) 15761–15785.

[2] S. Clough, M. W. Shepard, E. J. Mlawer, J. S. Delamere, M. J. Iacono, K. Cady-Pereira, S. Boukabara, P. D. Brown, Atmospheric radiative transfer modeling: a summary of the AER codes, Journal of Quantitative Spectroscopy and Radiative Transfer 91 (2005) 233–244.

[3] N. A. Scott, A. Chedin, A fast line-by-line method for atmospheric absorption computations: The automatized atmospheric absorption atlas, Journal of Applied Meteorologyr 20 (1981) 802–812.

[4] A. A. Lacis, V. Oinas, A description of the correlated k distribution method for modeling nongray gaseous absorption, thermal emission, and multiple scattering in vertically inhomogeneous atmospheres, Journal of Geophysical Research: Atmospheres 96 (D5) (1991) 9027–9063.

[5] C. J. Drummond, G. L. Stephens, A novel k-distribution parameter development system and its application to MAS/SUCCESS channels (1998).

[6] F. André, The ℓ-distribution method for modeling non-gray absorption in uniform and non-uniform gaseous media, Journal of Quantitative Spectroscopy and Radiative Transfer 179 (2016) 19–32.

[7] F. André, F. Coelho, J.-L. Consalvi, F. Franca, M. Galtier, F. Nmira, V. Solovjov, B. Webb, Accuracy of engineering methods for radiative transfer in CO2-H2O mixtures at high temperature, in: Proceedings of the 9th International Symposium on Radiative Transfer, RAD-19, Begellhouse, Connecticut, 2019, p. 407–414.

[8] M. Galtier, W. Woelffel, F. André, V. Solovjov, B. Webb, S. Roy, Assessment of engineering gas radiation methods in an industrial glass furnace configuration, in: submitted to the 8th European Thermal Sciences Conference, Lisbon, 2020.

[9] F. André, An analysis of the symmetry issue in the ℓ-distribution method of gas radiation in non-uniform gaseous media, Journal of Quantitative Spectroscopy and Radiative Transfer 190 (2017) 78–87.

[10] S. J. Young, Band model theory of radiation transport, Aerospace Press; American Institute of Aeronautics and Astronautics, 2013.

[11] R. A. McClatchey, R. W. Fenn, J. E. A. Shelby, F. E. Voltz, J. S. Garing, Optical properties of the atmosphere, Research paper AFCRF-72-0497, Hanscom Air Force Base (1972).

[12] F. André, A polynomial chaos approach to narrow band modeling of radiative heat transfer in non-uniform gaseous media, Journal of Quantitative Spectroscopy and Radiative Transfer 175 (2016) 17–29.

[13] W. L. Godson, The evaluation of infra-red radiative fluxes due to atmospheric water vapour, Quarterly Journal of the Royal Meteorological Society 79 (341) (1953) 367–379.

[14] S. J. Young, Nonisothermal band model theory, Journal of Quantitative Spectroscopy and Radiative Transfer 18 (1) (1977) 1–28.

[15] M. P. Weinreb, A. C. Neuendorffer, Method to apply homogeneous-path transmittance models to inhomogeneous atmospheres, Journal of the Atmospheric Sciences 30 (4) (1973) 662–666.

[16] L. L. Gordley, J. M. Russell, Rapid inversion of limb radiance data using an emissivity growth approximation, Applied optics 20 (5) (1981) 807–813.

[17] M. F. Modest, Narrow-band and full-spectrum k-distributions for radiative heat transfer—correlated-k vs. scaling approximation, Journal of Quantitative Spectroscopy and Radiative Transfer 76 (1) (2003) 69–83.

[18] B. T. Marshall, L. L. Gordley, D. A. Chu, BANDPAK: Algorithms for modeling broadband transmission and radiance, Journal of Quantitative Spectroscopy and Radiative Transfer 52 (5) (1994) 581–599.

[19] R. B. Nelsen, An introduction to copulas, Springer Science & Business Media, 2007.

[20] F. André, Effective scaling factors in non-uniform gas radiation modeling, Journal of Quantitative Spectroscopy and Radiative Transfer 204 (2018) 112–119.

[21] H. Joe, Multivariate models and multivariate dependence concepts, Chapman and Hall/CRC, 1997.

[22] J. Górecki, M. Hofert, M. Holena, An approach to structure determination and estimation of hierarchical Archimedean copulas and its application to bayesian classification, Journal of Intelligent Information Systems 46 (2016) 21–59.

[23] J. Górecki, M. Hofert, M. Holena, Kendall's tau and agglomerative clustering for structure determination of hierarchical Archimedean copulas, Special issue: Salzburg workshop onDependence Models and Copulas 5 (2017) 75–87.

[24] C. Hering, M. Hofert, J.-F. Mai, M. Scherer, Constructing hierarchical Archimedean copulas with Lévy subordinators, Journal of Multivariate Analysis 101 (6) (2010) 1428 – 1433.

[25] R. Schilling, R. Song, Z. Vondracek, Bernstein functions: theory and applications, Walter de Gruyter, 2012.

[26] C. Cornet, L. C.-Labonnote, F. Szczap, Three-dimensional polarized monte carlo atmospheric radiative transfer model (3DMCPOL): 3D effects of polarized visible reflectances of cirrus cloud, Journal of Quantitative Spectroscopy and Radiative Transfer 111 (1) (2010) 174–186.

[27] M. Rast, J. L. Bezy, S. Bruzzi, The ESA medium resolution imaging spectrometer MERIS: A review of the instrument and its mission, International Journal of Remote Sensing 20 (1999) 1681–1702.

[28] J. C. Buriez, C. Vanbauce, F. Parol, P. Goloub, M. Herman, B. Bonnel, al., Cloud detection and derivation of cloud properties from POLDER, International Journal of Remote Sensing 18 (1997) 2785–2813.

[29] I. Manolis, J. Caron, S. Grabarnik, J.-L. Bézy, M. Betto, H. Barré, G. Mason, R. Meynart, The MetOp second generation 3MI mission, Proceedings SPIE10564, International Conference on Space Optics - ICSO 2012 (2017).

[30] I. J. Barton, J. C. Scott, Remote measurement of surface pressure using absorption in the oxygen A-band, Applied Optics 25 (19) (1986) 3502–3507.

[31] P. Dubuisson, R. Borde, C. Schmechtig, R. Santer, Surface pressure estimates from satellite data in the oxygen A-band: Applications to the MOS sensor over land, Journal of Geophysical Research 106 (27) (2001) 277–286.

[32] H. Tran, C. Boulet, J.-M. Hartmann, Line mixing and collision-induced absorption by oxygen in the A band: Laboratory mesurements, model, and tools for atmospheric spectra computations, Journal of Geophysical Research 111 (2006).

[33] P. Dubuisson, J.-C. Buriez, Y. Fouquar, High spectral resolution solar radiative transfer in absorbing and scattering media: application to the satellite simulation, Journal of Quantitative Spectroscopy and Radiative Transfer 55 (1996) 103–126.

[34] C. Emde, V. Barlakas, C. Cornet, F. Evans, S. Korkin, Y. Ota, L. Labonnote, A. Lyapustin, A. Macke, B. Mayer, M. Wendisch, IPRT polarized radiative transfer model intercomparison project - phase A, Journal of Quantitative Spectroscopy and Radiative Transfer 164 (2015) 8–36.

[35] C. Emde, V. Barlakas, C. Cornet, F. Evans, W. Zhen, L. Labonnote, A. Macke, B. Mayer, M. Wendisch, IPRT polarized radiative transfer model intercomparison project - three-dimensional test case (phase B), Journal of Quantitative Spectroscopy and Radiative Transfer 209 (2018) 19–44.

[36] M. Desmons, N. Ferlay, F. Parol, L. Mcharek, C. Vanbauce, Improved information about the vertical location and extent of monolayer clouds from POLDER3 measurements in the oxygen A-band, Atmospheric Measurement Research 6 (8) (2010) 2221–2238.

[37] G. Merlin, J. Riedi, L. C.-Labonnote, C. Cornet, A. B. Davis, P. Dubuisson, M. Desmons, N. Ferlay, F. Parol, Cloud information content analysis of multi-angular measurements in the oxygen A-band: application to 3MI and MSPI, Atmospheric Measurement Technology 9 (10) (2016) 4977–4995.

[38] Z.-C. Zeng, F. Natraj, V.and Xu, T. J. Pongetti, R.-L. Shi, E. A. Kort, G. C. Toon, S. P. Sander, Y. L. Yung, Constraining aerosol vertical profile in the boundary layer using hyperspectral measurements of oxygen absorption, Geophysical Research Letters 45 (2018) 1–9.

[39] K. Stamnes, S. Tsay, W. Wiscombe, K. Jayaweera, Numerically stable algorithm for discrete-ordinate-method radiative transfer in multiple scattering and emitting layered media, Applied Optics 27 (12) (1988).